Dynamic light scattering studies of the aggregation of lysozyme under crystallization conditions

Mohammed Skouri[1,2], Michel Delsanti[1*], Jean-Pierre Munch[1], Bernard Lorber[2] and Richard Giegé[2]

[1]*Laboratoire d'Ultrasons et de Dynamique des Fluides Complexes, URA 851 du CNRS, Université Louis Pasteur, 4. rue Blaise Pascal, F-67070 Strasbourg Cedex* and [2]*Laboratoire de Biochimie, Institut de Biologie Moléculaire et Cellulaire du CNRS, 15. rue René Descartes, F-67084 Strasbourg Cedex, France*

The intensity autocorrelation functions of light scattered by lysozyme solutions under pre-crystalization conditions in NaCl-containing media were recorded at scattering angles from 20° to 90°. The measurements, conducted on freshly prepared protein solutions supersaturated more than 3-fold, indicate the simultaneous presence of two scatterer populations which can be assigned to individual protein molecules and to large particles. When solutions are undersaturated, or slightly supersaturated, light scattering only reveals the presence of the small scatterers. In the supersaturated medium, where aggregates were detected, lysozyme crystals grew in a time-span of 1–3 days after the scattering experiments. These results are correlated with the nucleation step during protein crystallization.

Dynamic light scattering; Protein; Lysozyme; Supersaturation; Aggregation; Crystallization

1. INTRODUCTION

The preparation of high quality crystals of biological macromolecules remains very often a limiting factor for the study of their three-dimensional structure by crystallographic methods. This fact relies in part on the lack of precise understanding of the physical chemistry of crystal growth, and particularly of the early aggregation and/or nucleation stage of the macromolecules. In the last years, dynamic light scattering (DLS) has become a popular method to approach this problem [1–10] because it is a sensitive technique to evaluate macromolecular interactions and detect formation of aggregates in solution [11,12]. Following these lines DLS has already been used, either as a diagnostic tool for the search of solvent conditions in which crystallization can occur [5,10] or for monitoring crystallization in supersaturated macromolecular solutions [4]. In the latter case hen egg white lysozyme was the model protein, supersaturation was induced by temperature, and the intensity autocorrelation function (ICF) of light scattered at 90° was recorded from the onset of supersaturation up to the growth of tetragonal lysozyme crys-

tals of noticeable size. It was found that the average diffusion coefficient of the protein in solution decreases to a minimum (i.e. the apparent size of the scatterers increases) as supersaturation proceeds, and increases up to its initial value as crystal growth takes place. Here, novel DLS experiments were performed on various lysozyme solutions whose compositions correspond to different parts of the crystal/solution phase diagram of the protein. The aggregation and/or nucleation state of the protein at the early stages of crystallization was evaluated by exploring scattering angles between 20 and 90° in the temperature range 5–20°C. Under conditions where crystallization takes places over a reasonable duration (1–3 days), DLS data on freshly prepared protein solutions indicate the presence of two scatterer populations corresponding to individual protein molecules and large aggregates. These results will be discussed within the framework of our present knowledge on the mechanism of protein crystal growth.

2. MATERIALS AND METHODS

2.1. Light scattering measurements

The beam provided by an argon ion laser (model Spectra Physics 2000; $\lambda = 488$ nm, 600 mV) was focused on the center of the cell containing the protein solution. Scattered light was collected at angles between 20 and 90°. More details on the instrumentation are given in [13]. For the best accuracy on measurements at small angles, cells with a large diameter (i.d. 88 mm) were used (to accommodate 1 ml samples) instead of the small cells employed for the conventional diagnostic measurements (performed at 90° on 80 μl samples) [5]. The digital autocorrelation function $g_2(t)$ was derived by a BI 30 or BI 80 correlator (Brookhaven Instruments, USA) and analyzed using the cumulant method [14] with:

$$g_2(t) = Ae^{-<\Gamma>t}|1 + \tfrac{1}{4}v^2 <\Gamma>^2 t^2| + B$$

In this equation $<\Gamma>$ is the average decay rate, t the time, v the variance that measures the deviation to a single exponential profile for a single relaxation process, and A and B constants. In order to obtain both $<\Gamma>$ and v, it was verified that B values coincide with the baseline calculated from $g_2(\infty)$. Also the presence of any potential scatterer distribution was searched by using different sample times to measure the autocorrelation function. The translational diffusion coefficient D of the scatterers was deduced from the average decay rate using the relation, $D = <\Gamma> / 2K^2$, where K is the scattering wavevector given by $K = (4\pi n/\lambda)\sin(\theta/2)$, where λ is the wavelength, n the refractive index and θ the scattering angle.

For a bimodal distribution of scatterers, the autocorrelation function can be written:

$$g_2(t) = |A_1 e^{-<\Gamma_1>t} + A_2 e^{-<\Gamma_2>t}|^2 + B$$

where A_1 and $<\Gamma_1>$ represent the amplitude and the decay rate of each contribution. When $<\Gamma_1>$ and $<\Gamma_2>$ are very different (as is the case here with $<\Gamma_1> / <\Gamma_2> \geq 100$) they can be measured separately. For very long sample times $(<\Gamma_1>t\rightarrow\infty)$, the contribution attributed to small scale motions is constant and the cumulant analysis described above can be used to determine $2<\Gamma_2>$. For very short sample times $(<\Gamma_2>t\rightarrow 0)$, where the contribution of the long scale motion is background, a cumulant analysis was used to fit the square root of the autocorrelation function $\sqrt{g_2(t)} - g_2(\infty)$, and to extract $<\Gamma_1>$ and A_2. For more details, see [12].

Assuming that scatterers are rigid spherical particles, the apparent hydrodynamic radius of the particles was calculated using the Stokes-Einstein relationship $R_h = k_B T/6 \pi \eta D$, where k_B is the Boltzmann constant, η the viscosity of the solvent and D the translational diffusion coefficient.

2.2. Preparation of solutions and crystallization procedure

Hen egg white lysozyme from Sigma (Cat. No. L-6876, lot No. 46F-80601) was dissolved in double-deionized water at 200 mg/ml and dialyzed at 20°C against 40 mM sodium acetate at pH 4.6. The solution was centrifuged (13 000 rpm, 10 min at 20°C) and the protein concentration of the supernatant determined spectrophotometrically using the extinction coefficient $0.38 \; A_{280 \; nm}$/mg/ml/cm. Dilutions (1 ml) containing 5, 10 or 20 mg/ml and 2, 3, 4 or 5% (w/v) NaCl and 40 mM sodium acetate at pH 4.6, were pipetted in light scattering cells and centrifuged (5000 rpm, 1 h) to clarify solutions from dust particles. Cells were placed in the thermostated bath of the DLS spectrophotometer and DLS measurements were performed 30 min after temperature was set. Supersaturation was induced by decreasing temperature by steps of 2°C/40 min. After measurements, samples were kept at the final temperature for up to 3 days to allow crystallization to occur. For instance, a sample containing 20 mg/ml lysozyme and 4% (w/v) NaCl crystallized in about 24 h at 10°C.

3. RESULTS AND DISCUSSION

We recall that crystal solubility curves in protein phase diagrams delineate regions of super- and under-saturation in which crystals are stable or in which they dissolve, respectively. The supersaturated region can further be divided into a zone of moderate to low super-saturation in which nucleation and hence crystal growth can occur (in time ranges going from minutes to months) and a zone of much higher supersaturation in which proteins form amorphous precipitates. Such phase diagrams depend upon protein and crystallizing agent concentrations, and the boundaries between the
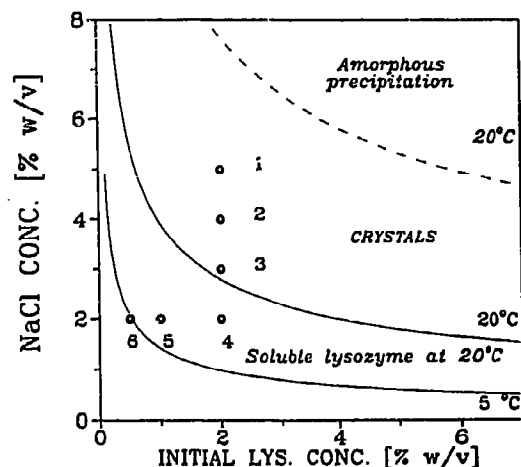

Fig. 1. Sample composition of the hen egg white lysozyme solutions used in DLS experiments and their location in a two-dimensional crystal/solution phase diagram of the protein. The variable parameters in the diagram are the initial concentrations of lysozyme and of NaCl (for pH values comprised between 4 and 5) (adapted from [17,26]). The 6 samples containing 4 different NaCl concentrations with a constant protein concentration (samples 1–4) or 3 different initial lysozyme concentrations with a constant the salt concentration (samples 4–6) are indicated. Solid lines represent the solubility limit at following temperatures: 5°C (from [26]) and 20°C (from [17]). The dashed line schematizes the boundary between the supersaturated region in which crystals are stable, and the region of amorphous precipitation, at 20°C (adapted from [27]).

different regions can be varied by many parameters including temperature (e.g. [15,16] and Fig. 1).

For a better understanding of the behaviour of lysozyme in the pre-crystallization regime, 6 solvent conditions at the boundary between super- and undersaturated regions in the protein phase diagram were investigated by DLS (Fig. 1). At 20°C, these conditions are such that samples are located either in the supersaturated region but close enough to the solubility curve so that neither nucleation or crystal growth is obtained in the 3-day period in which the experiments were carried out (samples 1, 2 and 3, with supersaturations up to 3 as calculated from data taken in [17]), or in the solubility domain where the protein solution is undersaturated (samples 4, 5 and 6). For all these solutions (at 20°C), the ICF was well described by a cumulant fit with a variance lower than 0.1 (i.e. a low polydispersity) in the whole range of scattering angles. As an example, the ICF for sample 4 in which lysozyme is slightly undersaturated, is displayed in Fig. 2A.

By lowering temperature (e.g. from 20 to 5°C), the samples with higher NaCl and lysozyme content (samples 1–4) enter deeply inside the supersaturated region (supersaturations up to 16). Under those conditions each ICF clearly exhibits a two-exponential decay as seen in Fig. 2B for sample 4.

The effect of the scattering wave-vector on the shape of ICFs provides information on the nature of relaxation processes. For instance, a linear K^2 dependence of
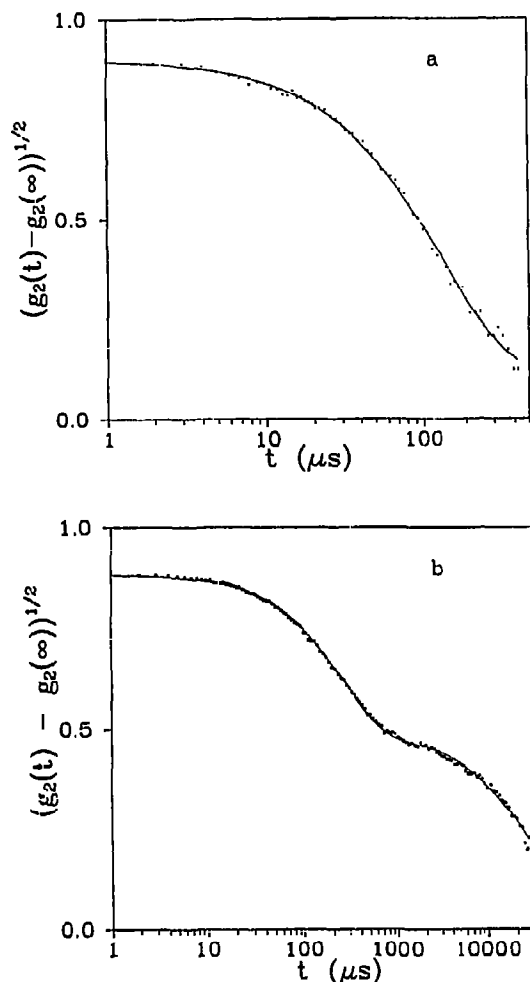
Fig. 2. Plot of the ICF of an (a) undersaturated and (b) supersaturated lysozyme solution as a function of time. Data correspond to the ICF of light scattered at 30° by sample 4: (a) at 20°C; (b) at 6°C.

Fig. 3. Plot of $<\Gamma>$ / K^2 vs. K^2 of the two decay processes observed in an ICF of a supersaturated lysozyme solution. Data were obtained with sample 4 at 6°C as in Fig. 2b.

the average decay rate $<\Gamma>$ is indicative of a diffusive process [12]. Therefore the variation of $<\Gamma>$ / K^2 relative to the two decay processes was investigated as a function of K^2. Fig. 3 shows that experimental data can be fitted with two horizontal lines, demonstrating that concentration fluctuations decay according to two diffusive processes. Furthermore, the amplitude relative to the slow mode increases considerably when K, in other words the scattering angle, decreases (results not shown).

The temperature at which the transition between the regime where the ICF can be satisfactorily described by a single cumulant fit and the regime characterized by a two-exponential decay was estimated on samples containing 20 mg/ml lysozyme and variable amounts of NaCl. ICF measurements were performed at low scattering angle (30°C) since the amplitude of the slow mode is higher at low K. As indicated in Fig. 4a, the transition curve divides the NaCl vs. temperature diagram into two regions where the ICFs exhibit either two
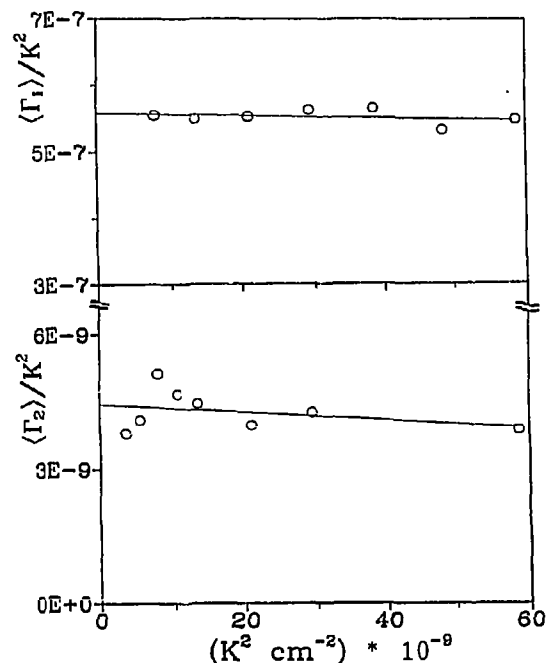
or one decay. This reflects the onset of an aggregation process occurring below a given temperature which is a function of the protein and crystallizing agent concentrations. This transition differs from the crystal/solution transition curve (Fig. 2b) in that the slow mode is only detected at higher NaCl concentrations for a given tem-
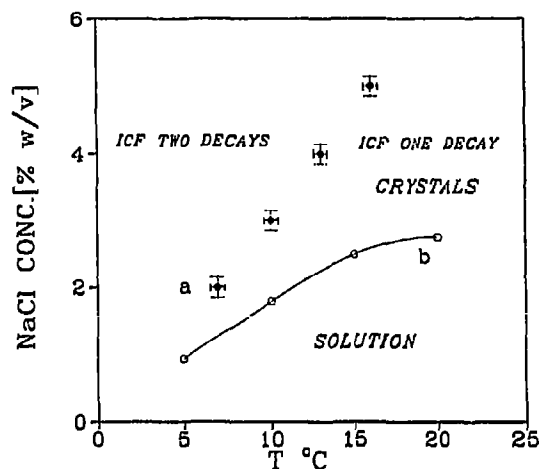

Fig. 4. Diagram of the crystallizing agent (NaCl) concentration vs. temperature for the transition (a) between one decay and two decays in ICFs and (b) between soluble and crystalline lysozyme for protein solutions with an initial concentration of 20 mg/ml at pH 4.6. DLS data (a) were obtained with samples 1–4; they are represented by crossed error bars (temperature ± 1°C; NaCl concentration ±5%). It should be recalled that the limits of detection of the slow decay mode are dependent upon experimental DLS conditions, so that the location of the DLS data in the diagram may change but probably without altering the trend of the transition curve.

perature. Interestingly, the two curves come closer to each other when temperature is lowered.

In summary, the present study gives evidence for the existence of two types of scatterers in lysozyme solutions under pre-crystallization conditions. This assumption is supported by the K^2 dependence of the decay rates. The apparent hydrodynamic radii of both types of particles calculated for sample 1 at 6°C are R_{h1} = 25 Å and R_{h2} = 2700 Å (under the assumption discussed in section 2). The value for R_{h1} is equal to that of individual protein monomers within the limits of experimental error (the radius calculated from the X-ray structure of the protein is 17 Å [18]). The value for R_{h2} is much larger and would correspond to clusters of thousands of monomers. The apparent discrepancy between these data and those from former measurements done at a 90° angle that revealed only one type of scatterers with a small hydrodynamic radius [4] is explained by the very faint contribution of the large size particles to the ICF at 90°C.

How can these results be related to the conclusions arising from former studies aimed to approach the problem of protein nucleation and how do they correlate with the current crystallization theories? For small molecules it is admitted that growth proceeds from stable nuclei having reached a critical size [19–22]. This size has been estimated by theoretical calculations, but up until now methodological difficulties hampered experimental verifications. Early estimates of the critical radius of chymotrypsinogen nuclei [23] were one order of magnitude lower than the apparent hydrodynamic radius R_{h2} found for the large aggregates of lysozyme. For other proteins, the interpretation of DLS measurements done at 90° has led to the proposal that much smaller particles (i.e. trimers of canavalin [6] and hexamers of insulin [9]) might be the primary aggregates in the course of their crystallization. This variability in the size of the putative nuclei of macromolecules is not in disagreement with data obtained with inorganic or small organic molecules. Indeed, calculated numbers of molecules in stable nuclei range from less than ten molecules to several thousand (e.g. [19–22]).

For proteins, it is presently not proven with certainty whether the aggregates observed under supersaturated conditions are nuclei, pre- or post-nucleation states, dead-end products or particles unrelated to crystallization. In the present case of lysozyme a body of observations strongly supports the idea that the aggregates seen by light scattering are involved in the crystallization process. Indeed in all cases where a slow mode was detected in ICF, macroscopic crystals were obtained in 1–3 days. Furthermore, recent DLS measurements conducted in the presence of ammonium sulphate in which lysozyme does not crystallize [24], have shown only one decay in the ICF corresponding to scatterers larger than monomers but smaller than the above aggregates [25]. Preliminary results have also indicated that the size of

the aggregates in NaCl containing solvents increases with time [25].

In this context, the existence of an intermediary region in the phase diagram, located between the ICF transition curve and the transition curve separating soluble and crystalline lysozyme, must be emphasized (see Fig. 4). This region is characterized by a low supersaturation (below 4) and the occurrence of a single decay in the ICFs. Also no macroscopic crystals were observed after 3 days under the experimental conditions defined in this intermediary region. This suggests the absence of significant nucleation and consequently it is tempting to postulate that the ICF transition curve delineates the supersaturation threshold (about 4–7 with lysozyme under the conditions investigated here) which must be overcome to achieve nucleation. If so, it can be assumed that the scatterers characterized by the slow decay rate are related to the nucleation process and that DLS could be a useful tool to define experimentally the metastable zone in which nucleation occurs in the phase diagram. From a more general point of view, biological macromolecules could be appropriate models for approaching yet unsolved phenomena in crystal growth, in particular nucleation, because their large size will favour experimentation dedicated to verify theories established for small molecules.

REFERENCES

[1] Kam, Z., Shore, H.B. and Feher, G. (1978) J. Mol. Biol. 123, 539–555.

[2] Baldwin, E.T., Crumley, K.W. and Carter, C.W. (1986) Biophys. J. 49, 47–48.

[3] Carter, J.W., Baldwin, E.T. and Frick, L. (1988) J. Crystal Growth 90, 60–73.

[4] Mikol, V., Hirsch, E. and Giegé, R. (1989) FEBS Lett. 258, 63–66.

[5] Mikol, V., Hirsch, E. and Giegé, R. (1990) J. Mol. Biol. 213, 187–195.

[6] Kadima, W., McPherson, A., Dunn, M.F. and Jurnak, F. (1990) Biophys. J. 57, 125–132.

[7] Auersch, A., Littke, W., Lang, and Burchard, W. (1991) J. Crystal Growth 110, 201–207.

[8] Bishop, J.B., Martin, J.C. and Rosenblum, W.M. (1991) J. Crystal Growth 110, 164–170.

[9] Kadima, W., McPherson, A., Dunn, M.F. and Jurnak, F. (1990) J. Crystal Growth 110, 188–194.

[10] Mikol, V., Vincendon, P., Eriani, G., Hirsch, E. and Giegé, R. (1991) J. Crystal Growth 110, 195–200.

[11] Candau, S. (1982) in: Surfactant Science vol. 22 (J. Zana ed.) pp. 147–207.

[12] Pecora, R. (1985) Dynamic Light Scattering, Plenum Press, New York.

[13] Candau, S. and Zana, J. (1981) J. Colloid Interface Sci. 84, 206–219.

[14] Koppel, D.E. (1972) J. Chem. Phys. 57, 4814–4820.

[15] Giegé, R. and Mikol, V. (1989) Trends Biotechnol. 7, 277–282.

[16] Ries-Kautt, M. and Ducruix, A. (1991) in: Crystallization of Nucleic Acids and Proteins: A Practical Approach (A. Ducruix and R. Giegé ed.) pp. 195–218. IRL, Oxford.

[17] Howard, S.B., Twigg, P.J., Baird, J.K. and Meehan, E.J. (1988) J. Crystal Growth 90, 94–104.

[18] Phillips, D.C. (1967) Proc. Natl. Acad. Sci. USA 57, 484–495.

[19] Mullin, J.W. (1961) Crystallization. Butterworths, London, p. 102.

[20] Chernov, A.A. (1984) Modern Crystallography III, Crystal Growth, Springer Verlag, Berlin, p. 61.

[21] Boistelle, R. (1986) in: Advances in Nephrology, vol 15 (Grünfeld, J.P., Maxwell, M.H., Bach, J.F., Crosnier, J. and Funck-Brentano, J.L. eds.) pp. 173–213, Yearbook Medical Publishers Inc., Chicago.

[22] Black, S.N. and Davey, R.J. (1988) J. Crystal Growth 90, 136–144.

[23] Hamilton, J.A., Koustky, J.A. and Walton, A.G. (1964) Nature 204, 1085–1086.

[24] Ries-Kautt, M. and Ducruix, A. (1989) J. Biol. Chem. 264, 745–748.

[25] Skouri, M., Munch, J.P., Lorber, B., Giegé, R. and Candau, S. (1991) Crystal Growth of Biological Macromolecules, A FEBS Advanced Lecture Course, (abstr.) Freiburg, Germany.

[26] Ataka, M. and Asai, M. (1988) J. Crystal Growth 90, 86–93.

[27] Feher, G. and Kam, Z. (1985) Methods Enzymol. 114, 77–112.